Chapter 22
Analyzing Anomalous Diffusion in NMR Using a Distribution of Rate Constants

R.L. Magin, Y.Z. Rawash, and M.N. Berberan-Santos

1 Introduction

There is a growing realization that relaxation and diffusion phenomena in complex materials cannot be expressed simply in terms of sum of exponential decays, each characterized by a single relaxation time or rate [8]. In nuclear magnetic resonance (NMR) and in optical luminescence studies, single-exponential models fail to describe the wide variety of relaxation times observed in synthetic and biological materials [6, 11]. In luminescence decay, for example, the observed relaxation spans many orders of magnitude – from nanoseconds to milliseconds – and a wide distribution of rate constants is needed to describe the phenomena [5]. In NMR relaxation experiments, the direct measurement of a distribution of T2 relaxation times from 1 to 1,000 ms is possible, but only for high signal-to-noise data collected from bulk samples [10]. The same is true for so-called q-space NMR diffusion measurements [1]. Our attention has been drawn recently to the success of simple empirical fits to the NMR diffusion attenuation in pulsed field gradient (PFG) studies [7], where both magnetic resonance imaging (MRI) and diffusion distribution analysis are possible. In PFG, the signal attenuation caused by diffusion can be measured for applied magnetic field gradients and the data fit to a simple-exponential decay law:

$$S(b) = S_0 \exp(-bD), \tag{22.1}$$

R.L. Magin (✉) • Y.Z. Rawash
Department of Bioengineering, University of Illinois at Chicago, 851 South Morgan Street, Chicago, IL, 60607–7052, USA
e-mail: rmagin@uic.edu; yrawas2@uic.edu

M.N. Berberan-Santos
Centro de Quimica-Fisica Molecular, Instituto Superior Tecnico, 1049–001, Lisboa, Portugal
e-mail: mbs@ist.utl.pt

D. Baleanu et al. (eds.), *Fractional Dynamics and Control*,
DOI 10.1007/978-1-4614-0457-6_22,

where b is a measure of the applied gradient strength and duration, and D is the effective diffusion constant, with units of mm^2/s. For high b-value experiments ($b > 1{,}000\mathrm{s}/\mathrm{mm}^2$) in the brain, however, the data collected from both gray and white matter do not follow a single exponential and have been simply fit using the so-called, stretched-exponential decay law:

$$S(b) = S_0 \exp\left[-(bD_\alpha)^\alpha\right], \tag{22.2}$$

where $0 < \alpha < 1$ and D_α is the fractional diffusion constant. A rationale for the empirical function was recently provided using fractional calculus [6,11,14,18]. The purpose of this chapter is to show that the stretching parameter, α, directly reflects a "distribution" of many single-exponential relaxation rates. This analysis follows closely the approach used by [3] in applying the stretched exponential and similar functions to the time decay of optical luminescence signals.

2 Underlying Distributions

The exponential function (22.1) can also be written in a more general form. Let $I(b) = S(b)/S_0$, so we can write:

$$I(b) = \exp\left(-\int_0^b w(u)\mathrm{d}u\right), \tag{22.3}$$

where $w(b)$ is a b-value-dependent rate coefficient, defined by:

$$w(b) = -\frac{\mathrm{d}\ln I(b)}{\mathrm{d}b} = -\frac{1}{I(b)}\frac{\mathrm{d}I(b)}{\mathrm{d}b}. \tag{22.4}$$

In the simplest case, $w(b)$ can be b-value independent with, for example, $w(b) = D$ and the decay is an exponential function as in (22.1). Equation (22.3) can be easily generalized to fractional order as follows:

$$I(b) = \exp\left(-\left[1 * w(b)\right]\right) = \exp\left(-\left[k_\alpha(b) * w(b)\right]\right). \tag{22.5}$$

Here, the $*$ symbol indicates the convolution operator and $k_\alpha(b)$ is a monotonically decreasing function that provides fading memory of earlier b-values. If we assume that we can write $k_\alpha(b)$ as a power law, $k_\alpha(b) = b^{\alpha-1}/\Gamma(\alpha)$, where $\Gamma(\alpha)$ is the γ function, then (22.5) takes the form of a classical Riemann–Liouville fractional integral [9], and we have:

$$I(b) = \exp\left(-I_0^\alpha[w(b)]\right). \tag{22.6}$$

Now in the case of $w(b) = D$, we find using either the properties of fractional calculus or the Laplace transformation, that:

$$I(b) = \exp\left[-b^{\alpha} D/\Gamma(\alpha)\right] = \exp\left[-(bD_{\alpha})^{\alpha}\right], \tag{22.7}$$

where $D_{\alpha} = D/\Gamma(1+\alpha)$ is the effective diffusion constant and the diffusion decay curve is a stretched-exponential function of b.

The relaxation function $I(b)$ used to describe diffusion signal attenuation is thus seen to span the range from a single exponential to a stretched exponential depending upon the amount of memory included in the convolution; with longer memory, additional, slower components of the response could be expected to become more evident. Another way of spanning both long and short diffusion components is to assume two or more single exponentials are present. This is the usual approach to incorporate multi-compartmental and multi-component behavior. Here we will take this idea to the extreme and assume a distribution of exponential terms that can also be written as:

$$I(b) = L\left[\rho\left(k_{\mathrm{D}}\right)\right] = \int_0^{\infty} \rho\left(k_{\mathrm{D}}\right) \mathrm{e}^{-bk_D} \mathrm{d}k_{\mathrm{D}}. \tag{22.8}$$

This relation is valid as long as the integral exists (i.e. $\rho(k_{\mathrm{D}})$ grows no faster than an exponential) and shows $\rho(k_{\mathrm{D}})$ to be the inverse Laplace transform of $I(b)$. The function $\rho(k_{\mathrm{D}})$ is normalized, as $I(0) = 1$ implies:

$$\int_0^{\infty} \rho\left(k_{\mathrm{D}}\right) \mathrm{d}k_{\mathrm{D}} = 1. \tag{22.9}$$

The integrand of (22.8), $\rho(k_{\mathrm{D}}) \exp(-bk_{\mathrm{D}})$, can be seen as a particular diffusion term in the distribution with k_{D} viewed either as the corresponding diffusion coefficient or as the rate constant for the process that proceeds with advancing b.

In previous work, we found that the stretched-exponential function is well suited to describe signal attenuation caused by diffusion phenomena in gels, cartilage, and brain tissue [11]. We now will show that the distribution of rate constants – the probability density function – outlined above for a stretched-exponential function is well suited to describe and characterize intrinsic properties of the complex environment that water inhabits in each of these cases.

Recovery of the distribution $\rho(k_{\mathrm{D}})$ from experimental data is an ill-conditioned problem [12]. In other words, a small change in $I(b)$ can cause an arbitrarily large change in $\rho(k_{\mathrm{D}})$. In general, high signal-to-noise is needed so that $\rho(k_{\mathrm{D}})$ can be recovered from the experimental relaxation decay results. A simple form of the inverse Laplace transform of a relaxation function can be obtained by the

method outlined by [3]. Briefly, the three following equations can be used for the computation of $\rho(k_D)$ from $I(b)$:

$$\rho(k_D) = \frac{2}{\pi} \int_0^\infty \mathrm{Re}\left[I(i\omega)\right] \cos(k_D \omega)\, \mathrm{d}\omega \tag{22.10}$$

$$\rho(k_D) = -\frac{2}{\pi} \int_0^\infty \mathrm{Im}\left[I(i\omega)\right] \sin(k_D \omega)\, \mathrm{d}\omega \tag{22.11}$$

$$\rho(k_D) = \frac{1}{\pi} \int_0^\infty \mathrm{Re}\left[I(i\omega)\right] \sin(k_D \omega)\, \mathrm{d}\omega - \mathrm{Im}\left[I(i\omega)\right] \sin(k_D \omega)\, \mathrm{d}\omega. \tag{22.12}$$

3 Anomalous Diffusion Model

The stretched-exponential model follows from a fundamental extension of the Bloch–Torrey equation through application of the operators of fractional calculus [11]. This promising model needs further investigation and study; however, like models of [2] and of [7], it describes the anomalous diffusion behavior of signal attenuation using a stretched-exponential function. The specific formula derived by Magin et al. is:

$$I(b) = \exp\left[-D\mu^{2(\beta-1)} (\gamma G_z \delta)^{2\beta} \left(\Delta - \frac{2\beta - 1}{2\beta + 1}\delta\right)\right]. \tag{22.13}$$

In this equation, γ is the gyromagnetic ratio for the water proton (42.58 MHz/T), G_z is the spatial gradient in z direction, Δ is the time between the two gradient pulses, δ is the gradient pulse duration, and D is the diffusion coefficient. In this model there are also two fractional order-related parameters: μ, a space constant needed to maintain consistent units and β, the order of the fractional calculus operator, $0.5 < \beta \leq 1$, which can be related to the complexity of the material.

For the case of $\beta = 1$, the classic expression for diffusion is recovered, that is:

$$I(b) = \exp\left[-D(\gamma G_z \delta)^2 (\Delta - \delta/3)\right]. \tag{22.14}$$

Using (22.13) the theoretical curves are plotted in Fig. 22.1, as $I(b)$ versus the gradient parameter b (where for $\Delta \gg \Delta$, $b = (\gamma G_z \delta)^2 \delta$) for selected values of μ and β. In this figure a gradient pulse sequence G_z, Δ, and δ is assumed with G_z varying from 0 to 1,500 mT/m. We observe that as β decreases from 1.0 to 0.6, the attenuation curves change from a simple exponential (a straight line on the semi-log

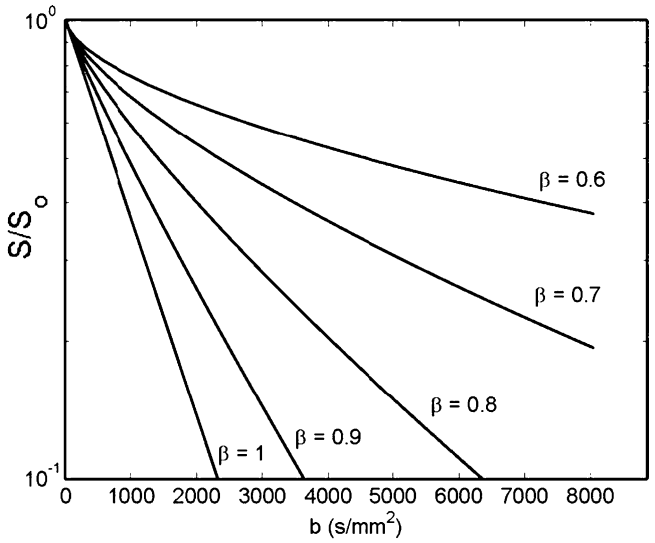

Fig. 22.1 Normalized signal attenuation decay (22.13), plotted versus b, where $b = (\gamma G_z \delta)^2 \Delta$, for selected values of β. In each curve, G_z increases from 0 to 1,500 mT/m while all other parameters are fixed: $D(1 \times 10^{-3}\,\mathrm{mm^2/s})$, Δ (50 ms), δ (1 ms), and μ(35μm)

graph) to heavy-tailed curved shape that strongly resembles the behavior recorded in restricted diffusion – particularly at high b-values.

In Fig. 22.2, (22.13) is plotted for a series of μ-values ranging from 20 to 80μm with $\beta = 0.8$. The G_z, Δ, and δ-values in Fig. 22.2 are the same as those used in Fig. 22.1. Here we see that increasing the value of μ appears to increase the contribution of restricted diffusion in the diffusion attenuation curve for a fixed value of β. This behavior is evident when (22.13) is expressed either in terms of a single-exponential decay, $\exp\{-bD_{\mathrm{apI}}\}$, where the apparent diffusion coefficient is expressed as:

$$D_{\mathrm{apI}} = D/((\gamma G_z \delta)\mu)^{2(1-\beta)}, \tag{22.15}$$

or when (22.13) is written as a stretched exponential, $\exp\{-(bD_{\mathrm{F}})^{\beta}\}$, where:

$$D_{\mathrm{F}}^{\beta} = D\left(\Delta/\mu^2\right)^{1-\beta}. \tag{22.16}$$

In addition, when $\mu = \sqrt{D\Delta}$, (22.13) corresponds with the "stretched exponential" result, $\exp\{-(bD)^{\beta}\}$, considered by [2]. In the example plotted in Fig. 22.2 this correspondence occurs for $\mu = 7.07$μm. Overall, Figs. 22.1 and 22.2 show for (22.13) a decrease in the apparent diffusion coefficient as the values of β decrease and values of μ increase.

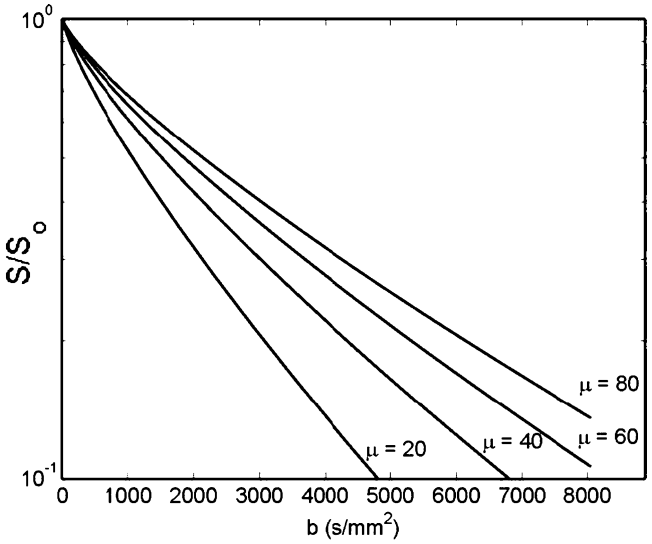

Fig. 22.2 Normalized signal attenuation decay (22.13), plotted versus b, where $b = (\gamma G_z \delta)^2 \Delta$, with selected values of μ. In each curve, G_z increases from 0 to 1,500 mT/m while all other parameters are fixed: $D(1 \times 10^{-3}\,\mathrm{mm^2/s})$, Δ (50 ms), δ (1 ms), and β (0.8)

4 Anomalous Distribution Model

The stretched-exponential decay function was also recently used in the analysis of single-molecule fluorescence, quantum dot luminescence, and in the fluorescence lifetime imaging of biological tissues [6]. The determination of $\rho(k_\mathrm{D})$ for a given $I(b)$ amounts to finding the inverse Laplace transform of the stretched-exponential decay function.

The result, first obtained by [15], and an equivalent integral representation found by [3], is:

$$\rho(k_\mathrm{D}) = \frac{1}{\pi D_\mathrm{F}} \int_0^\infty \mathrm{e}^{-u^\beta \cos\left(\frac{\beta\pi}{2}\right)} \cos\left(u^\beta \sin\left(\frac{\beta\pi}{2}\right) - \frac{k_\mathrm{D} u}{D_\mathrm{F}}\right) \mathrm{d}u. \tag{22.17}$$

In addition, a convergent power series for $\rho(k_\mathrm{D})$ is known:

$$\rho(k_\mathrm{D}) = \frac{1}{\pi D_\mathrm{F}} \sum_{n=1}^{\infty} \frac{(-1)^{n+1}}{n!} \frac{\sin(n\beta\pi)}{(k_\mathrm{D}/D_\mathrm{F})^{(1+n\beta)}} \Gamma(1+n\beta). \tag{22.18}$$

It can be seen that the asymptotic form of $\rho(k_\mathrm{D})$ is:

$$\rho(k_\mathrm{D}) = \frac{\Gamma(1+\beta)}{\pi D_\mathrm{F}} \frac{\sin(\beta\pi)}{(k_\mathrm{D}/D_\mathrm{F})^{1+\beta}}. \tag{22.19}$$

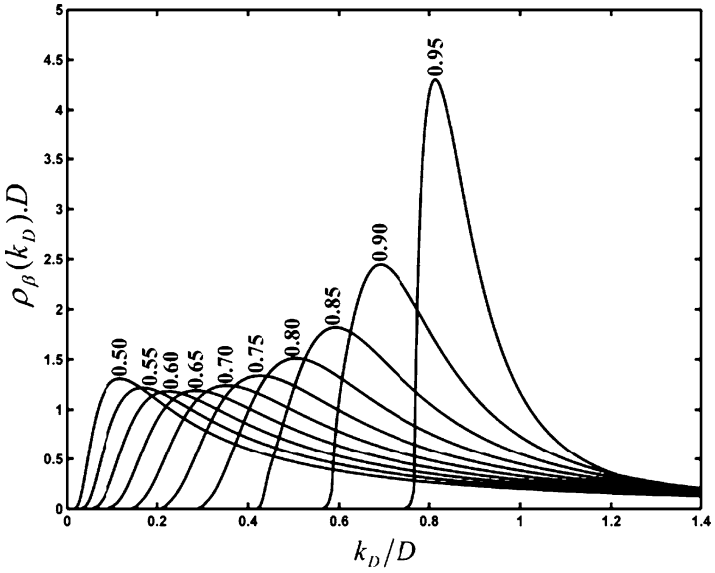

Fig. 22.3 A series of plots of the distribution of diffusional decay rates calculated using (22.18). The β-values span the range from 0.5 to 0.95

We have calculated the distribution of diffusional rate constants $\rho(k_{\mathrm{D}})$ using (22.18) for a range of β-values from 0.5 to 0.95, and the results are plotted in Fig. 22.3. As the value of β approaches 1, the distribution appears to converge toward a Dirac Delta function corresponding to a single-exponential function with $k_{\mathrm{D}} = D$, whereas, as β approaches the value of 0.5, the distribution of diffusional relaxation rates broadens and becomes more uniform. A similar broadening of the distribution occurs for a fixed value of β as μ is increased, as is shown in Fig. 22.4.

The stretched-exponential decay function is necessarily of an approximate nature, as it implies an infinitely fast initial rate of decay. Super-exponential short-time behavior results from the fat tail of the stretched-exponential distribution [4]. Usually, one is, however, more interested in the long-time behavior, which is governed by the shape of the distribution of rate constants near the origin. With this aim in view, an exponentially attenuated modified form of the stretched-exponential distribution was proposed [4]. The resulting decay law retains the original long-time behavior but no longer suffers from the short-time problems of the original distribution. Other well-behaved decay functions that encompass the exponential function as a special case such as the compressed hyperbola have been proposed and successfully applied to several problems where a continuous distribution of rate constants was found to exist [16, 17].

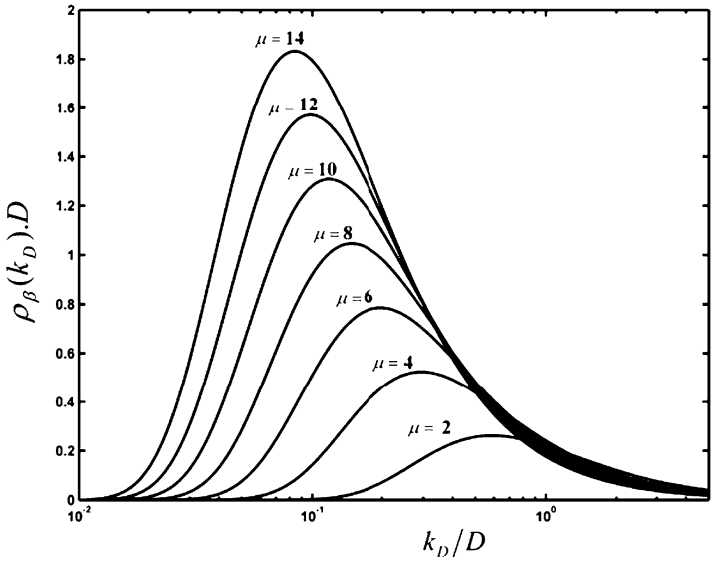

Fig. 22.4 A series of plots of the distribution of diffusional decay rates calculated using (22.18) with β of 0.5. The μ-values span the range from 2 to 14μm

5 Experimental Results

Two diffusion-weighted MRI (DWI) experiments were carried out at 11.74 T (500 MHz for protons) to illustrate applications of the stretched-exponential model to characterized biological complexity. In first experiment, glass capillary tubes were filled with Sephadex (Sigma-Aldrich, St. Louis, MO) gels type G-25, G-50, and G-100, and placed in a 5 mm NMR tube filled with distilled water. Diffusion-weighted images were acquired using a Stejskal–Tanner diffusion-weighted spin–echo pulse sequence with the following parameters: TR = 1,000 ms, TE = 60 ms, slice thickness = 1.5 mm, Δ = 45 ms, δ = 1 ms, and 4 averages. The FOV was 0.6 cm × 0.6 cm, which for a matrix size of 64 × 64 corresponds to an in-plane resolution of 94 μm × 94 μm.

In the second experiment, diffusion-weighted brain imaging was carried out on a healthy human volunteer at the University of Illinois Medical Center. Axial images were acquired with multiple *b*-values using a customized single-shot EPI. The key data acquisition parameters were: TR = 4,000 ms, TE = 96.6 ms, slice thickness of 4 mm, slice gap of 3 mm, Δ = 42.6 ms, δ = 32.2 ms, and 4 averages. Diffusion-weighted images were acquired with a maximum *b*-value of 3,300 s/mm^2.

The signal attenuation results from DWI for the two experiments (Figs. 22.5 and 22.6) was measured for selected regions of interest (ROI) at increasing *b*-values,

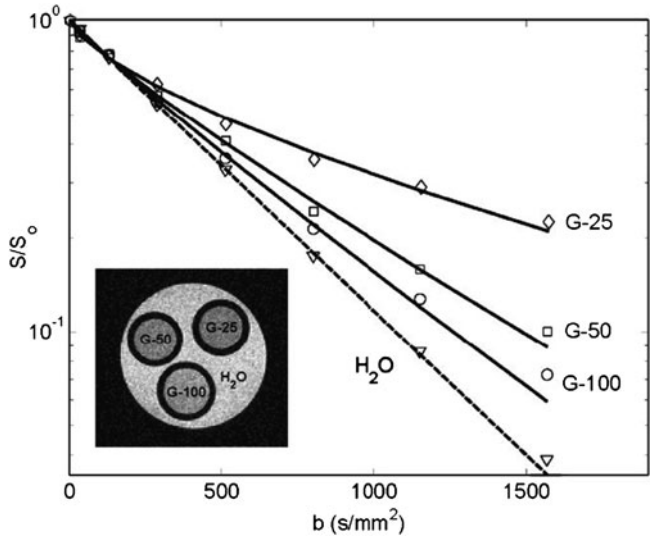

Fig. 22.5 Normalized signal intensity plotted versus b, where $b = (\gamma G_z \delta)^2 \Delta$, for selected ROI in samples of distilled water and Sephadex G-25, G-50, and G-100. The experimental data were fit to the fractional-order model (22.13) to determine D_F, β, and μ

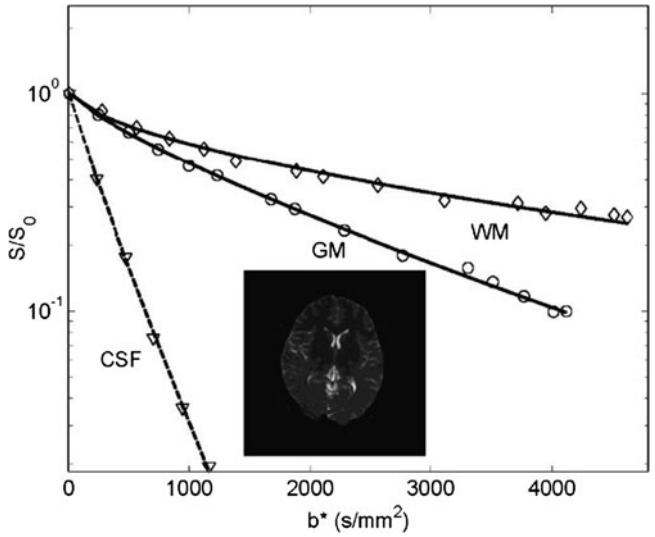

Fig. 22.6 Normalized signal intensity plotted versus b^*, from (22.13) for selected ROI in white matter, gray matter and cerebrospinal fluid for a human brain. The experimental data were fit to the fractional-order stretched-exponential model. (22.13) for D, β, and μ, where $b^* = (\gamma G_z(\delta)^2(\Delta - ((2\beta - 1)/(2\beta + 1))\delta)$

Table 22.1 Diffusion and complexity measurement

	$D_F \times 10^{-3}$ mm^2/s	β (a.u.)	μ(μm)
G-25	1.1 ± 0.04	0.71 ± 0.06	6.4 ± 0.1
G-50	1.5 ± 0.03	0.8 ± 0.05	5.7 ± 0.1
G-100	1.8 ± 0.06	0.91 ± 0.08	4.4 ± 1.6
Distilled water	2.1 ± 0.02	1.0 ± 0.003	2.9 ± 0.3
White matter	0.41 ± 0.006	0.60 ± 0.008	4.3 ± 0.04
Gray matter	0.75 ± 0.08	0.78 ± 0.03	4.9 ± 0.02
CSF	2.8 ± 0.18	0.91 ± 0.005	3.0 ± 1.3

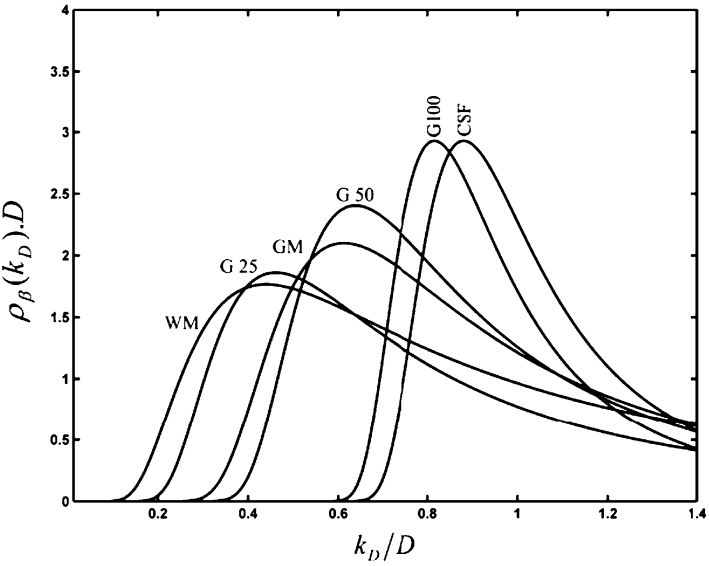

Fig. 22.7 Distribution of rate constants (probability density function) calculated using (22.18) for the stretched-exponential relaxation function for (Sephadex G-25, G-50 and G-100, CSF, gray matter, and white matter)

and the data fit to the stretched-exponential model (22.13) using the Levenberg–Marquardt nonlinear least squares algorithm. A summary of the results is listed in Table 22.1.

We have used (22.18) to calculate the distribution of diffusional rate constants $\rho(k_D)$ for the data on Sepadex gels (Fig. 22.5) and for human brain tissue (Fig. 22.6). The resulting distributions are plotted in Fig. 22.7. The results provide a graphic depiction of the effect of the fractional-order parameter β to embed a wide range of diffusion rates. As expected, the water and water-like cerebral spinal fluid (CSF) have very narrow distributions while the Sephadex gels, beginning with the G-100 (largest pore size) fan out with decreasing G-number (effectively the gel's molecular exclusion value in kilodaltons). Interestingly, the gray matter distribution peaks between the G-25 and G-50 Sephadex samples, while the white matter shows an almost uniform distribution of diffusion rates.

6 Discussion and Conclusions

In this work, we demonstrated that a stretched-exponential model describing anomalous diffusion in disordered system can be employed with success to characterize the diffusion results from the MR signal attenuation curves obtained from Sephadex gels and biological tissue during DWI experiments. Moreover, the probability density function of diffusional rate constants was found to describe and characterize the complexity of gels and biological tissue in a manner consistent with the water distribution inside the biological environments.

The general properties and conditions of the MR signal attenuation curves were outlined for the MR signal in order to have a probability density function of rate constants; it was concluded that the decay must be either exponential or sub-exponential for all b-values, if $\rho(k_{\mathrm{D}})$ is to be a probability density function. The use of the stretched-exponential model for analyzing MR signal attenuation curves has been shown to provide excellent tissue discrimination [11, 18]. Even more importantly, the stretched-exponential function not only describes the decay profiles almost exactly but also derives from the more realistic decay model of continuous distributions in biological tissue, rather than from an arbitrary assumption of single or multiple discrete exponential decay components.

The heterogeneity parameter β is important because it enables the study of mechanisms that cause a continuous distribution to broaden or narrow. Future work on a variety of different tissue types and in different environmental conditions will hopefully provide more insight in this matter. It is possible that the heterogeneity parameter β is sensitive to the gradient direction, particularly in highly anisotropic structures in the brain. This is expected because diffusion imaging of the brain has revealed considerable anisotropy. In the present studies, diffusion gradients were applied in only one direction to avoid averaging the data in more than one direction. Results showed reduced μ in regions of human brain corresponding to the superior sagittal sinus. This is thought to occur because of partial volume effects between the relatively fast-diffusing CSF in the sinus and the slow-diffusing gray matter parenchymal protons and white matter in between, so it is likely that μ can be related to the porosity and tortuosity in biological tissue, and more specifically to the heterogeneity of the biological tissue.

A stretched-exponential model that describes diffusion in a random disordered system and fractal spaces was used to parameterize the diffusion and biological complexity from diffusion-weighted MR signals. The model performed well on data obtained from Sephadex gel type G-100, G-50, and G-25 as well as on data from human brain tissues (white and gray matter) with different predicted diffusion characteristics. This approach has potential to be applied in clinical studies and may aid in monitoring the developmental as well as pathological changes to biological tissues.

Acknowledgment The authors R.L. Magin and Y.Z. Rawash would like to acknowledge the support of NIH grant R01 EB007537.

References

1. Assaf Y, Cohen Y (2000) Assignment of the water slow-diffusing component in the central nervous system using q-space diffusion MRS: implications for fiber track imaging. Magn Reson Med 43: 191–199
2. Bennett KM, Schmainda KM, Bennett RT, Rowe DB, Lu H, Hyde JS (2003) Characterization of continuously distributed cortical water diffusion rates with a stretched exponential model. Magn Reson Med 50:727–734
3. Berberan-Santos MN (2005) Analytical inversion of the Laplace transform without contour integration: Application to luminescence decay laws and other relaxation functions. J Math Chem 38:165–173
4. Berberan-Santos MN, Bodunov EN, Valeur B (2005) Mathematical functions for the analysis of luminescence decays with underlying distributions 1. Kohlrausch decay function (stretched exponential). J Lumin 126:263–272
5. Berberan-Santos MN, Valeur B (2007) Luminescence decays with underlying distributions: General properties and analysis with mathematical functions. 1. Kohlrausch decay function (stretched exponential). Chem Phys 315:171–182
6. Berberan-Santos MN, Bodunov EN, Valeur B (2008) Luminescence decays with underlying distributions of rate constants: General properties and selected cases. In Bereran-Santos MN (ed) Fluorescence of supermolecules, polymers, and nanosystems. Springer, Berlin, pp 105–116
7. Hall MG, Barrick TR (2008) From diffusion-weighted MRI to anomalous diffusion imaging. Magn Reson Med 59:447–455
8. Hilfer R (2002) Applications of fractional calculus in physics. World Scientific, Singapore
9. Kilbas AA, Srivastava HM, Trujillo JJ (2006) Theory and applications of fractional differential equations. Elsevier, Amsterdam
10. Lin PC, Reiter DA, Spencer RG (2009) Classification of degraded cartilage through multi-parametric MRI analysis. J Magn Reson 201:61–71
11. Magin RL, Abdullah O, Baleanu D, Zhou XJ (2008) Anomalous diffusion expressed through fractional order differential operators in the Bloch–Torrey equation. J Magn Reson 190: 255–270
12. Mollay B, Kauffman HF (1994) Dynamics of energy transfer in aromatic polymers. In: Richert R, Blumen A (eds) Disorder effects on relaxational processes: glasses, polymers, proteins. Springer, Berlin, pp 509–541, 509
13. Narayanan A, Hartman JS, Bain AD (1995) Characterizing nonexponential spin–lattice relaxation in solid-state NMR by fitting to the stretched exponential. J Magn Reson Ser A 112:58–65
14. Peled S, Cory DG, Raymond SA, Kirschner DA, Jolesz FA (1999) Water diffusion, T_2, and compartmentation in frog sciatic nerve. Magn Reson Med 42:911–918
15. Pollard K (1946) The representation of $\exp(-x^{\alpha})$ as a Laplace integral. Bull Amer Math Soc 52:908–910
16. Souchon V, Leray I, Berberan-Santos MN, Valeur B (2009) Multichromophoric supramolecular systems. Recovery of the distributions of decay times from the fluorescence decays. Dalton Trans 20:3988–3992
17. Whitehead L, Whitehead R, Valeur B, Berberan-Santos MN (2009) A simple function for the description of near-exponential decays: The stretched or compressed hyperbola. Am J Phys 77:173–179
18. Zhou XJ, Gao Q, Abdullah O, Magin RL (2010) Studies of anomalous diffusion in the human brain using fractional order calculus. Magn Reson Med 63:562–569